

# Learn Structure, Adapt on the Fly: Multi-Scale Residual Learning and Online Adaptation for Aerial Manipulators

Samaksh Ujjawal<sup>1</sup>, Naveen Sudheer Nair<sup>1</sup>, Shivansh Pratap Singh<sup>1</sup>, Rishabh Dev Yadav<sup>2</sup>, Wei Pan<sup>2</sup>, Spandan Roy<sup>1</sup>

**Abstract**—Autonomous Aerial Manipulators (AAMs) are inherently coupled, nonlinear systems that exhibit nonstationary and multiscale residual dynamics, particularly during manipulator reconfiguration and abrupt payload variations. Conventional analytical dynamic models rely on fixed parametric structures, while static data-driven models assume stationary dynamics and degrade under configuration changes and payload variations. Moreover, existing learning architectures do not explicitly factorize cross-variable coupling and multi-scale temporal effects, conflating instantaneous inertial dynamics with long-horizon regime evolution. We propose a predictive-adaptive framework for real-time residual modeling and compensation in AAMs. The core of this framework is the Factorized Dynamics Transformer (FDT), which treats physical variables as independent tokens. This design enables explicit cross-variable attention while structurally separating short-horizon inertial dependencies from long-horizon aerodynamic effects. To address deployment-time distribution shifts, a Latent Residual Adapter (LRA) performs rapid linear adaptation in the latent space via Recursive Least Squares, preserving the offline nonlinear representation without prohibitive computational overhead. The adapted residual forecast is directly integrated into a residual-compensated adaptive controller. Real-world experiments on an aerial manipulator subjected to unseen payloads demonstrate higher prediction fidelity, accelerated disturbance attenuation, and superior closed-loop tracking precision compared to state-of-the-art learning baselines, all while maintaining strict real-time feasibility.

## I. INTRODUCTION

Autonomous Aerial Manipulators (AAMs) integrate a quadrotor or multirotor drone with a robotic arm. This setup boosts the drone’s dexterity and versatility, enabling tasks from basic payload transport to advanced operations like pick-and-place, contact inspection, grasping, and assembly [1], [2]. Nevertheless, this integration introduces fundamentally challenging dynamics that defy classical analytical treatment such as configuration-dependent inertia variations as the arm moves or engages the environment (e.g., during grasping or dropping, see Fig. 1), nonlinear coupling forces between the drone and arm, and aerodynamic phenomena, such as rotor downwash and manipulator-induced flow interference [3], [4]. These forces collectively dominate system behavior, making it diverge from assumed mathematical model and giving rise to *residual dynamics*.

Conventional AAM control methods [3]–[5] rely on analytical knowledge of the underlying system model. Unfortunately, it is difficult, if at all possible, to accurately represent

configuration-dependent inertial coupling forces analytically [3, Ch.5.3]. Therefore, these traditional control frameworks struggle to compensate for residual dynamics. Data-driven methods [6], [7] have recently found footprints in robotics literature to tackle the issues that arise from model-based methods. However, these existing methods are not directly suitable for the residual dynamics in an AAM system. In the following, we steer our discussion in this direction.



Fig. 1: Aerial manipulation platform consisting of a quadrotor and a 2-DOF robotic arm transporting different payloads.

## A. Related Works

Offline data-driven models such as Deep Neural Networks (DNNs) [8], [9], Gaussian Processes (GPs) [10], [11], Physics-Informed Temporal Convolutional Networks (TCNs) [12], Recurrent Neural Networks (RNNs) [13], NeuralSDEs [14] and Diffusion [15] have been found effective for quadrotors. While expressive beyond analytic models, offline models trained on static datasets perform poorly for AAM under time-varying dynamics caused by manipulator reconfiguration and payload changes, leading to accumulating prediction errors and degraded control without online adaptation [6].

Recent work addresses nonstationary and time-varying disturbances by adapting [16] or updating the dynamics model [7], [17]–[20]. Several deep learning-based approaches update only the final layer via gradient descent [17] requiring careful optimizer tuning and exhibiting poor sample efficiency under limited data. Others periodically retrain the full network and merge parameters using an exponential moving average [7], incurring substantial computational overhead. Meta-learning methods [16], [19] interpolate among pre-trained models, thereby limiting extrapolation to previously unseen dynamics. While GP regression [18], Bayesian last-layer adaptation [19], and adaptive control

<sup>1</sup>Robotics Research Center, International Institute of Information Technology Hyderabad, Hyderabad, India

<sup>2</sup>Department of Computer Science, The University of Manchester, U.K.

schemes [20] enable online updates, they do not explicitly separate cross-variable coupling from multi-scale temporal effects, such as fast configuration-dependent inertial interactions and slower aerodynamic or payload-induced transients. Moreover, these methods typically assume gradual and sufficiently data-rich adaptation regimes and do not explicitly address multi-scale residual dynamics. The structural requirements motivating our design are discussed below.

*a) Multiscale Dynamics:* Residual dynamics in AAMs exhibit a multi-scale structure: fast components from configuration-dependent inertial coupling and Coriolis effects, and slower components from aerodynamic wake interactions and payload-induced inertia redistribution [4], [21]. The former depend on the instantaneous state, whereas the latter evolve over multiple control cycles due to physical time constants. Capturing both requires short-horizon history (e.g., 1–5 samples) for fast coupling and longer windows (e.g.,  $\geq 5$ –20 samples) for slowly varying regimes. Standard Transformers do not explicitly separate these temporal scales.

*b) Spatial Tokenization:* Conventional time-tokenized Transformers emphasize dependencies across time steps, whereas AAM residual dynamics are primarily governed by cross-variable coupling across degrees of freedom. Consequently, temporal attention conflates instantaneous spatial interactions with long-horizon regime memory, lacking inductive bias aligned with the underlying physics.

*c) Online Adaptation:* Payload changes and aggressive maneuvers require adaptation to streaming data without retraining the entire network or compromising high-frequency control stability. This demands decoupling offline nonlinear representation learning from lightweight online parameter identification, which generic Transformer frameworks do not inherently support.

Taken together, effective residual modeling for aerial manipulators demands structured factorization across variables, temporal scales, and adaptation modes. To address these requirements, we propose a predictive–adaptive framework (cf. Fig. 3) with the following contributions:

- 1) **Structure-Aligned Residual Modeling:** We introduce the Factorized Dynamics Transformer (FDT), a dual-stream architecture that treats physical variables as tokens rather than time steps. This induces attention across physical variables while structurally separating short-horizon interactions from long-horizon regime memory.
- 2) **Latent Linear Online Identification:** We propose a Latent Residual Adapter (LRA) that restricts online adaptation to a linear correction in latent space, updated via Recursive Least Squares. This preserves the offline nonlinear representation while enabling rapid adaptation without modifying the backbone network.
- 3) **Residual-Compensated Adaptive Control Integration:** The adapted residual prediction is incorporated into an adaptive control law to compensate modeling error in closed loop. The resulting controller avoids full knowledge or identification of system model and adapts for a single parameter irrespective of system

complexity, avoiding any computational burden.

The proposed framework aligns architectural structure with the physical characteristics of aerial manipulator residual dynamics, enabling accurate prediction and principled online adaptation. We validate the approach on a real aerial manipulator platform under unseen payload conditions, demonstrating improved prediction fidelity, faster disturbance recovery, and real-time feasibility in closed-loop operation.

## II. METHODOLOGY

We consider a quadrotor-based AAM composed of a 6-degrees-of-freedom (DOF) floating base and an  $n_{arm}$ -DOF robotic arm. Let  $n \triangleq 6 + n_{arm}$  denote the total number of generalized coordinates, and let  $\chi \in \mathbb{R}^n$  be the full configuration vector with control input  $\tau \in \mathbb{R}^n$ . The system dynamics follow the Euler–Lagrange formulation [3], [21]

$$M(\chi)\ddot{\chi} + C(\chi, \dot{\chi})\dot{\chi} + g(\chi) + d(\dot{\chi}, t) = \tau, \quad (1)$$

where  $M(\chi) \in \mathbb{R}^{n \times n}$  is the inertia matrix,  $C(\chi, \dot{\chi})\dot{\chi}$  represents Coriolis and centripetal effects,  $g(\chi)$  denotes gravity, and  $d(\dot{\chi}, t)$  captures aerodynamic and external disturbances.

To isolate configuration-dependent and nonstationary effects, we introduce a user-defined constant diagonal matrix  $\bar{M} \in \mathbb{R}^{n \times n}$  and rewrite (1) as

$$\bar{M}\ddot{\chi} + \mathbf{r}(\chi, \dot{\chi}, \ddot{\chi}, t) = \tau, \quad (2)$$

where the *residual dynamics* are defined as  $\mathbf{r} \triangleq (M(\chi) - \bar{M})\ddot{\chi} + C(\chi, \dot{\chi})\dot{\chi} + g(\chi) + d(\dot{\chi}, t)$ . The residual  $\mathbf{r}$  aggregates inertial coupling, nonlinear interaction forces, aerodynamic transients, and external disturbances into a single term. Rather than estimating each physical component separately, we directly learn  $\mathbf{r}$ , which is more suitable for aerial manipulators operating under continuously varying posture and payload conditions. From logged data, the residual can be computed as  $\mathbf{r}_t = \tau_t - \bar{M}\ddot{\chi}_t$ , allowing supervised learning from measured trajectories.

Given a history window of length  $T$ , we define the trajectory segment  $\mathcal{D}_t = \{(\chi_{t-i}, \dot{\chi}_{t-i}, \tau_{t-i})\}_{i=0}^T$ . Our objective is to learn a parameterized predictor that produces multi-step residual forecasts  $\hat{\mathbf{r}}_{t+j|t}$ , representing the  $j$ -step-ahead prediction conditioned on data available up to time  $t$ . The predictor is parameterized by  $\theta$  and maps  $\mathcal{D}_t$  to the prediction horizon. The model parameters  $\theta$  are obtained by minimizing the multi-step prediction loss

$$\mathcal{L}(\theta) = \sum_t \sum_{j=0}^k \|\mathbf{r}_{t+j} - \hat{\mathbf{r}}_{t+j|t}\|_2^2. \quad (3)$$

This multi-step objective reduces error accumulation during rollout and improves the stability of downstream control by encouraging accurate residual forecasts over the prediction horizon. The residual process  $\mathbf{r}_t$  depends on configuration-dependent inertial coupling and aerodynamic transients, introducing history-dependent effects not captured by a first-order Markov model. We adopt a two-stage strategy:

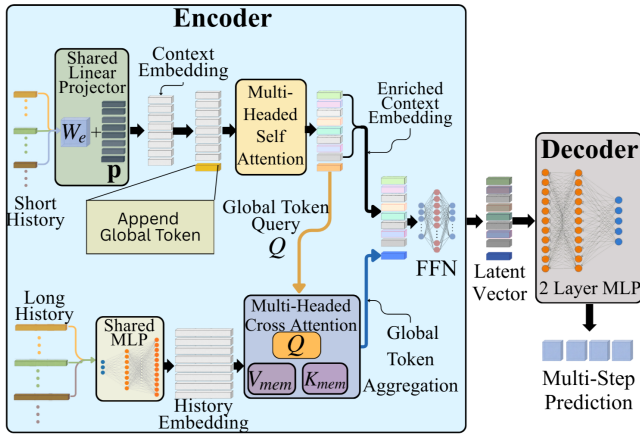


Fig. 2: The Factorized Dynamics Transformer (FDT) architecture. A dual-stream encoder separates short-horizon inertial coupling (via Self-Attention) from long-horizon aerodynamic memory (via Cross-Attention). A learnable Global Token aggregates both temporal scales into a unified Latent Vector, which is mapped to multi-step residual predictions by an MLP decoder.

- 1) **Offline Residual Learning:** Factorized Dynamics Transformer (FDT) is trained to approximate the mapping from  $\mathcal{D}_t$  to  $\{\hat{\mathbf{r}}_{t+j|t}\}_{j=0}^k$  using large-scale trajectory data.
- 2) **Online Latent Adaptation:** To handle distribution shifts induced by payload or operating-condition changes, a lightweight linear correction layer is adapted online in latent space using Recursive Least Squares (RLS).

This separation yields a residual predictor that is both high-capacity and computationally efficient for real-time aerial manipulation.

### A. Offline Residual Dynamics Learning

The residual process  $\mathbf{r}_t$  defined in (2) depends on configuration-dependent inertial coupling and aerodynamic transients, introducing both cross-variable interactions and history-dependent effects. Standard Markov models that rely solely on the instantaneous state  $(\chi_t, \dot{\chi}_t)$  are therefore insufficient to capture this structure. To model these multi-scale dependencies, we propose the **Factorized Dynamics Transformer (FDT)** (depicted in Fig. 2), a transformer-based architecture designed to (i) explicitly model inter-variable coupling and (ii) incorporate long-horizon temporal memory without recurrent state compression.

1) *Variable-Wise Temporal Embedding:* At each time step, the stacked input vector is  $\mathbf{x}_t = [\chi_t^\top \ \dot{\chi}_t^\top \ \tau_t^\top]^\top \in \mathbb{R}^{3n}$ . We therefore define the number of scalar input channels as  $d_v = 3n$ . Let  $z_{i,t}$  denote the  $i$ -th scalar component of  $\mathbf{x}_t$ . For each scalar variable  $i \in \{1, \dots, d_v\}$ , we extract its short-horizon history over  $T_s$  steps:

$$\mathbf{z}_i = [z_{i,t-T_s+1} \ \dots \ z_{i,t}]^\top \in \mathbb{R}^{T_s}. \quad (4)$$

Rather than tokenizing along the time dimension, each physical variable is treated as an independent token. Each token

is embedded into a latent space of dimension  $d_{model}$  via

$$\mathbf{e}_i = W_e \mathbf{z}_i + \mathbf{p}_i, \quad W_e \in \mathbb{R}^{d_{model} \times T_s}, \quad (5)$$

where  $W_e$  is shared across variables and  $\mathbf{p}_i \in \mathbb{R}^{d_{model}}$  is a learnable embedding encoding the physical identity of variable  $i$ . Stacking all embeddings yields the context matrix

$$E_{ctx} = \begin{bmatrix} \mathbf{e}_1 \\ \vdots \\ \mathbf{e}_{d_v} \end{bmatrix} \in \mathbb{R}^{d_v \times d_{model}}. \quad (6)$$

2) *Short-Horizon Context Encoding:* To capture instantaneous cross-variable dependencies relevant for control, we append a learnable global token  $\mathbf{g} \in \mathbb{R}^{d_{model}}$  to the context matrix:  $[E_{ctx}; \mathbf{g}] \in \mathbb{R}^{(d_v+1) \times d_{model}}$ . Multi-head self-attention (MSA) utilizing  $n_{heads}$  parallel attention heads is then applied to the updated context matrix

$$\tilde{E} = \text{MSA}([E_{ctx}; \mathbf{g}]) + [E_{ctx}; \mathbf{g}]. \quad (7)$$

The output can be partitioned as  $\tilde{E} = [\tilde{E}_{ctx}; \tilde{\mathbf{g}}_{ctx}]$ , where  $\tilde{\mathbf{g}}_{ctx}$  denotes the updated global token from the context branch. Since self-attention computes pairwise interactions across all tokens, the global token aggregates contextual information from all physical variables, forming a compact latent summary of the joint system state within the short-horizon window. While the attention mechanism does not enforce physical coupling explicitly, the variable-wise tokenization provides an inductive bias that encourages the model to learn dependencies across degrees of freedom.

3) *Long-Horizon Memory Retrieval:* Residual dynamics also exhibit slower temporal effects (e.g., wake interaction and payload-induced inertia shifts). To incorporate longer memory without quadratic self-attention over the entire sequence, we introduce a long-horizon window  $T_\ell > T_s$ . Simply increasing  $T_s$  would require applying full self-attention over longer temporal contexts, leading to quadratic growth in computational cost and potentially mixing instantaneous dynamics with slowly evolving regime effects. The proposed factorization instead separates these roles: short-horizon attention captures rapid cross-variable interactions, while long-horizon memory provides a compressed representation of slower aerodynamic and payload-induced dynamics.

Let the stacked long-horizon input sequence be

$$\mathbf{Z}_\ell = [\mathbf{x}_{t-T_\ell+1} \ \dots \ \mathbf{x}_t]^\top \in \mathbb{R}^{T_\ell \times d_v} \quad (8)$$

We use *Variable-Wise Temporal Embedding* as discussed in Section II-A.1, where the  $i$ -th token  $\mathbf{z}_i \in \mathbb{R}^{T_\ell}$ ,  $i = 1, \dots, d_v$ , carries the full long-horizon temporal history of the  $i$ -th state variable.

A single shared MLP with output embedding dimension  $d_{model}$  is applied identically to every variable token:

$$\mathbf{e}_i = \text{MLP}(\mathbf{z}_i) \in \mathbb{R}^{d_{model}}, \quad i = 1, \dots, d_v. \quad (9)$$

Stacking the embeddings yields long-horizon memory matrix

$$\mathbf{E}_{hist} = [\mathbf{e}_1 \ \dots \ \mathbf{e}_{d_v}]^\top \in \mathbb{R}^{d_v \times d_{model}} \quad (10)$$

Memory keys and values are obtained by projecting from  $d_{model}$  to  $d_k$ :

$$K_{mem} = \mathbf{E}_{hist} W_K \in \mathbb{R}^{d_v \times d_k}, \quad V_{mem} = \mathbf{E}_{hist} W_V \in \mathbb{R}^{d_v \times d_k}, \quad (11)$$

where  $W_K, W_V \in \mathbb{R}^{d_{model} \times d_k}$  are learnable projection matrices.

The updated global token  $\tilde{\mathbf{g}}_{ctx} \in \mathbb{R}^{d_{model}}$  serves as the query:

$$Q = \tilde{\mathbf{g}}_{ctx} W_Q \in \mathbb{R}^{1 \times d_k}, \quad W_Q \in \mathbb{R}^{d_{model} \times d_k}. \quad (12)$$

Cross-attention over the  $d_v$  physical-variable tokens yields

$$\alpha = \text{Softmax} \left( \frac{QK_{mem}^\top}{\sqrt{d_k}} \right) \in \mathbb{R}^{1 \times d_v}, \quad \mathbf{g}'_{ctx} = \alpha V_{mem} \in \mathbb{R}^{d_k}, \quad (13)$$

where the Softmax is applied across the  $d_v$  variable tokens, producing an attention weight that reflects the relative dynamical relevance of each physical channel over the long horizon.

This operation compresses the long-horizon trajectory into a single latent vector  $\mathbf{g}'_{ctx} \in \mathbb{R}^{d_k}$ , which acts as a low-dimensional representation of the current dynamic regime and is passed directly to the RLS adaptation stage as  $\mathbf{g}'_t$ .

4) *Residual Prediction*: The memory-enriched global token  $\mathbf{g}'_{ctx}$  encapsulates both short-horizon cross-variable interactions and long-horizon regime information is appended with to the context embedding from the MSA and we get the final encoder output embedding as :

$$\tilde{E}_{enc} = [E_{ctx}; \mathbf{g}'_{ctx}] \quad (14)$$

As shown in the decoder block of Fig. 2, this enriched context is passed through a position-wise feed-forward network (FFN) with a hidden expansion dimension of  $d_{ff}$ , followed by a multi-layer perceptron to produce multi-step residual predictions:

$$\mathbf{h} = \text{FFN}(\tilde{E}_{enc}), \quad \{\hat{\mathbf{r}}_{t+j|t}\}_{j=0}^k = \text{MLP}(\mathbf{h}). \quad (15)$$

The parameters of the FDT are trained offline by minimizing the loss in (3) over a dataset spanning diverse configurations, velocities, and payload conditions.

### B. Online Latent Residual Adaptation

While the offline FDT captures structured residual dynamics from diverse training data, aerial manipulators frequently experience distribution shifts caused by unseen payloads or abrupt operating-condition changes. To enable rapid adaptation without full-network retraining, we introduce a lightweight latent correction mechanism operating on the learned regime representation.

1) *Additive Latent Residual Model*: Let  $\hat{\mathbf{r}}_{t|t}^{base} \in \mathbb{R}^n$  denote the one-step residual prediction produced by the frozen FDT. From the encoder, we extract the memory-enriched global token  $\mathbf{g}'_t \in \mathbb{R}^{d_k}$ , which represents a compact latent embedding of the current dynamic regime.

We assume that deviations from the base model induced by payload or regime shifts are linear-in-parameters with respect to the latent feature:

$$\mathbf{r}_t = \hat{\mathbf{r}}_{t|t}^{base} + W^\top \mathbf{g}'_t + \varepsilon_t, \quad (16)$$

where  $W \in \mathbb{R}^{d_k \times n}$  is an adaptation matrix and  $\varepsilon_t \in \mathbb{R}^n$  denotes residual modeling error. The adapted residual prediction is therefore

$$\hat{\mathbf{r}}_{t|t}^{adapted} = \hat{\mathbf{r}}_{t|t}^{base} + W_t^\top \mathbf{g}'_t. \quad (17)$$

This structure preserves the expressive nonlinear mapping learned offline while restricting online adaptation to a linear correction in latent space.

2) *Recursive Least Squares Update*: The adaptation matrix  $W_t$  is updated online using Recursive Least Squares (RLS). Define the innovation error  $\varepsilon_t = \mathbf{r}_t - \hat{\mathbf{r}}_{t|t}^{adapted}$ .

Let  $\Sigma_t \in \mathbb{R}^{d_k \times d_k}$  denote the covariance matrix and  $\lambda \in (0, 1]$  a forgetting factor. The RLS update equations are

$$K_t = \frac{\Sigma_{t-1} \mathbf{g}'_t}{\lambda + \mathbf{g}'_t^\top \Sigma_{t-1} \mathbf{g}'_t}, \quad (18a)$$

$$W_t = W_{t-1} + K_t \varepsilon_t^\top, \quad (18b)$$

$$\Sigma_t = \frac{1}{\lambda} \left( \Sigma_{t-1} - K_t \mathbf{g}'_t^\top \Sigma_{t-1} \right). \quad (18c)$$

This update minimizes the exponentially weighted least-squares objective

$$\sum_{\tau=0}^t \lambda^{t-\tau} \|\mathbf{r}_\tau - \hat{\mathbf{r}}_{\tau|\tau}^{base} - W^\top \mathbf{g}'_\tau\|_2^2. \quad (19)$$

3) *Adaptive Covariance Reset*: A known limitation of standard Recursive Least Squares (RLS) is covariance collapse ( $\Sigma_t \rightarrow 0$ ), which gradually reduces parameter plasticity and slows adaptation when the system experiences abrupt regime shifts. In practice, this effect can cause the estimator to become overly confident in outdated parameters, preventing rapid adjustment to new dynamics such as sudden payload changes or aerodynamic disturbances.

To mitigate this issue, we introduce an adaptive covariance reset mechanism that restores estimator responsiveness when large prediction errors are observed. Let  $\bar{\varepsilon}_t$  denote the exponential moving average of the innovation error. If  $\|\bar{\varepsilon}_t\|_2 > \delta_{thresh}$ , the covariance matrix is reinitialized as  $\Sigma_t \leftarrow \sigma_0 I$ , where  $\sigma_0 > 0$  controls the adaptation aggressiveness and  $I$  is the identity matrix.

This reset temporarily increases the Kalman gain  $K_t$ , allowing the estimator to rapidly remap the latent feature  $\mathbf{g}'_t$  to the updated residual distribution. In effect, the mechanism restores estimator plasticity and enables fast adaptation under sudden dynamic changes. While this modification departs from the strict optimality guarantees of classical RLS, it acts as a practical safeguard that improves adaptation speed and robustness in the presence of nonstationary dynamics.

### C. Residual-Compensated Adaptive Control

While the FDT and LRA bring the nominal model closer to reality, a estimation error inevitably remains. Given the multi-step residual forecast  $\{\hat{\mathbf{r}}_{t+j|t}\}_{j=0}^k$  produced by the proposed learning framework, only the one-step prediction  $\hat{\mathbf{r}}_{t|t}$  is used for feedback compensation. After online adaptation, let  $\hat{\mathbf{r}}_{t|t}^{adapted}$  denote the corrected estimate and  $\sigma(t) \triangleq \hat{\mathbf{r}}_{t|t}^{adapted}(t) - \mathbf{r}(t)$ , bounded over a compact set, represents

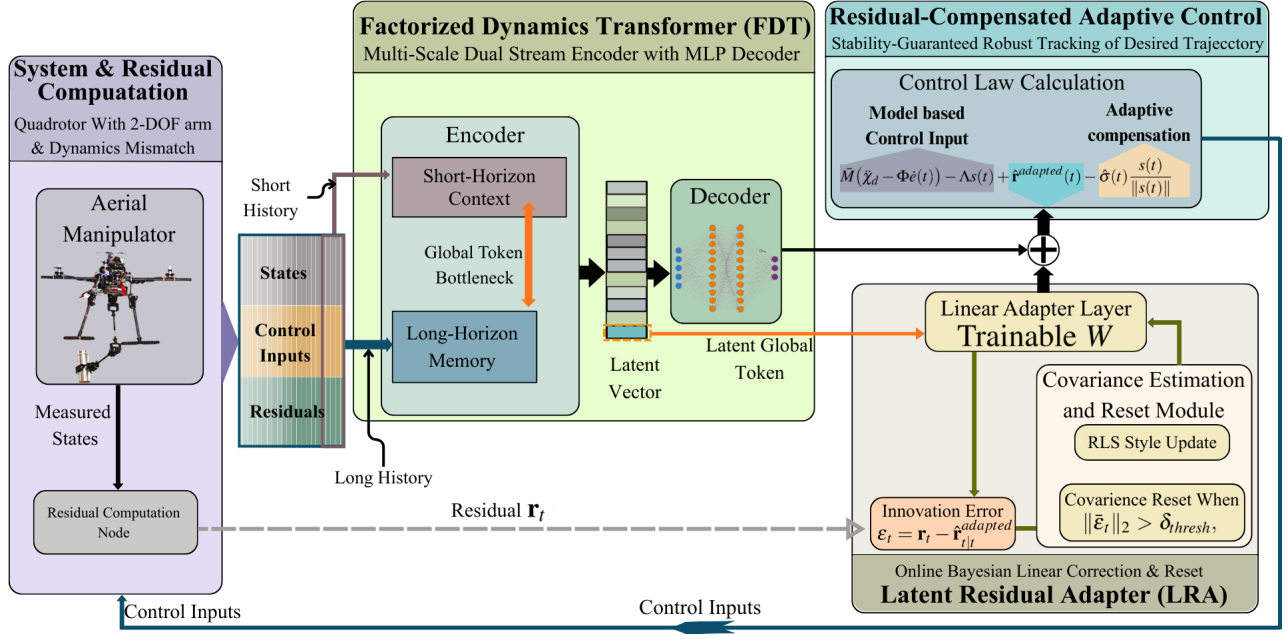


Fig. 3: The framework fuses a physics-aware **Factorized Dynamics Transformer (FDT)** with an online **Latent Residual Adapter (LRA)**. The FDT (center) utilizes inverted variable embeddings and a global-token bottleneck to efficiently compress long-horizon aerodynamic memory. To handle unmodeled regime shifts (e.g., payload changes), the LRA (bottom-right) performs online Bayesian correction directly on the frozen global token features, injecting a real-time adjustment into the adaptive control law (top-right) to guarantee robust trajectory tracking.

the residual estimation error. Denoting the tracking error as  $e(t) \triangleq \chi(t) - \chi_d(t)$ , where  $\chi_d(t)$  being the desired reference trajectory, we define an error variable  $s$  as

$$s(t) = \dot{e}(t) + \Phi e(t), \quad (20)$$

where  $\Phi \in \mathbb{R}^{n \times n}$  is a user-defined positive definite gain matrix. Multiplying the time derivative of (20) by  $\bar{M}$  and using (2) we obtain

$$\bar{M}\dot{s} = \bar{M}(\ddot{\chi} - \ddot{\chi}_d + \Phi\dot{e}) = \tau - \mathbf{r} - \bar{M}(\ddot{\chi}_d - \Phi\dot{e}). \quad (21)$$

We propose the following residual-compensated control law:

$$\tau(t) = \bar{M}(\ddot{\chi}_d - \Phi\dot{e}(t)) - \Lambda s(t) + \hat{\mathbf{r}}^{adapted}(t) - \hat{\sigma}(t) \frac{s(t)}{\|s(t)\|}, \quad (22a)$$

$$\dot{\hat{\sigma}}(t) = \|s(t)\| - \nu \hat{\sigma}(t), \quad \hat{\sigma}(0) > 0, \quad (22b)$$

where  $\Lambda \in \mathbb{R}^{n \times n}$  ( $\Lambda \succ 0$ ) is a control gain matrix,  $\nu > 0$  is a design constant, and  $\hat{\sigma}(t)$  is an adaptive gain designed to counteract bounded residual estimation uncertainties  $\sigma$ . Substituting the proposed control input (22a) back into open-loop dynamics (21) yields the closed-loop error dynamics:

$$\begin{aligned} \bar{M}\dot{s} &= -\Lambda s(t) + (\hat{\mathbf{r}}^{adapted}(t) - \mathbf{r}(t)) - \hat{\sigma}(t) \frac{s(t)}{\|s(t)\|} \\ &= -\Lambda s(t) + \sigma(t) - \hat{\sigma}(t) \frac{s(t)}{\|s(t)\|}. \end{aligned} \quad (23)$$

By continuously fine-tuning the latent representation via the online adapter, the magnitude of the estimation error  $\sigma(t)$  is drastically minimized. This proactively reduces the burden on the high-frequency adaptive term  $\hat{\sigma}(t) \frac{s}{\|s\|}$ , mitigating

#### Algorithm 1 Real-Time Residual-Compensated Control

**Input:** History  $\mathcal{D}_t$ , frozen FDT,  $\bar{M}$ ,  $(\lambda, \sigma_0, \delta_{\text{thresh}})$ ,  $(\Phi, \Lambda, \nu)$   
**Initialize:**  $W_0 = 0_{d_k \times n}$ ,  $\Sigma_0 = \sigma_0 I$ ,  $\hat{\sigma}(0) > 0$ ,  $\bar{\epsilon}_0 = 0$

- 1: **while** system active at time  $t$  **do**
- 2: Measure  $(\chi_t, \dot{\chi}_t, \ddot{\chi}_t)$  and append  $\mathcal{D}_t \leftarrow \chi_t, \dot{\chi}_t, \tau_t$
- 3: Compute residual  $r_t$  via (2)
- 4:  $(g'_t, \hat{r}_{t|t}^{base}) \leftarrow \text{FDT}(\mathcal{D}_t)$  // II-A
- 5:  $\epsilon_t \leftarrow r_t - (\hat{r}_{t|t}^{base} + W_{t-1}^\top g'_t)$  // (16)
- 6: Update  $(K_t, W_t, \Sigma_t)$  via RLS (18a)-(18c)
- 7: **If**  $\|\bar{\epsilon}_t\|_2 > \delta_{\text{thresh}}$  **Then**  $\Sigma_t \leftarrow \sigma_0 I$  // II-B.3
- 8:  $\hat{r}_{t|t}^{adapted} \leftarrow \hat{r}_{t|t}^{base} + W_t^\top g'_t$  // (17)
- 9: Compute  $s(t)$  via (20)
- 10: Update  $\hat{\sigma}(t)$  via (22b)
- 11: Apply control  $\tau(t)$  via ((22a)
- 12: **end while**

chattering and ensuring tight tracking precision. Algorithm 1 and Figure 3 summarize the closed-loop pipeline.

*Remark:* Although a unified end-to-end proof is not derived here, stability can be argued from established results under standard assumptions. The offline residual learner converges in the supervised learning sense given sufficiently rich training data; the Recursive Least Squares update yields bounded parameter estimates under persistent excitation and bounded noise; and the residual-compensated adaptive controller ensures Lyapunov stability under bounded residual estimation error.

### III. EXPERIMENTAL VALIDATION

We evaluate the proposed framework under realistic uncertainties to examine: (i) predictive fidelity and closed-loop tracking performance, (ii) the impact of latent-space adaptation via LRA during dynamic variations, and (iii) the structural contribution of each architectural component through ablation analysis.

#### A. Experimental Setup

1) *Hardware Platform*: For experimental validation, we built an aerial manipulator comprising a Tarot-650 quadrotor base (SunnySky V4006 motors, 14-inch propellers) and a 2-DOF planar serial-link manipulator (link lengths  $\approx 18$  cm) actuated by Dynamixel XM430-W210-T motors. The full system weighs  $\approx 3.0$  kg. The quadrotor is equipped with a CUAUV X7+ flight controller running customized PX4 firmware, while high-level FDT inference and Adaptive Control (AC) execution happens on an onboard NVIDIA Jetson Orin Nano (8GB). Sensor data from OptiTrack motion capture system (at 120 fps) and IMU were used to measure the necessary pose (position, attitude), velocity and acceleration feedback of the drone. For the manipulator, the joint angular position and velocity are measured by the Dynamixel motors, while the accelerations are computed numerically. Communication leverages Micro XRCE-DDS for low-latency uORB topic exchange, and the manipulator is controlled via the *ros2\_control* Joint Trajectory Controller. The resulting body moments and collective thrust commands are transmitted to flight controller at 50 Hz.

2) *Dataset Collection*: To collect diverse training data, we employ a baseline PID controller to execute randomized trajectories that heavily excite the coupled dynamics of the platform and manipulator. Data are gathered under three payload conditions (0 g, 200 g, 400 g) to generate configuration- and load-dependent inertial variations. For each condition, 5 minutes of data are recorded at 100 Hz, forming the raw time-indexed dataset  $\mathcal{D}_{\text{raw}} = \{(\chi^{(i)}, \dot{\chi}^{(i)}, \ddot{\chi}^{(i)}, \tau^{(i)})\}_{i=1}^{N_{\text{raw}}}$ .

3) *Implementation Details*: The FDT employs  $N_{\text{layers}} = 2$  encoder layers with latent dimension  $d_{\text{model}} = 512$  and  $n_{\text{heads}} = 8$ . The decoder is a 2-layer MLP with hidden width  $d_{\text{ff}} = 2048$ , projecting the latent representation before a final linear mapping to the residual dimension. The short- and long-horizon windows are set to  $T_s = 5$  and  $T_l = 120$  timesteps, respectively. The model performs  $k$ -step-ahead residual prediction ( $k = 6$ ) and is trained using the multi-step residual loss defined in (3) with the Adam optimizer (learning rate  $10^{-3}$ , batch size 256) for 100 epochs with validation-based early stopping. Online adaptation via LRA employs RLS with forgetting factor  $\lambda = 0.99$  and initial covariance  $P_0 = I$ . Covariance reset uses  $\delta_{\text{thresh}} = 3.2$ ,  $\sigma_0 = 1$ , and exponential smoothing factor  $\alpha = 0.9$ . The gain parameters are listed in Table I, where ‘diag’ denotes diagonal matrix. The desired roll and pitch of the quadrotor are calculated via [22]. For all learned models, the input features consist of the current state  $\chi_t$ , its velocity  $\dot{\chi}_t$ , and the previous control input  $\tau_{t-1}$ , since  $\tau_t$  is not available at prediction time [8].

TABLE I: Controller Parameter Settings

$\Phi = \text{diag}\{1.0, 1.0, 1.5, 1.1, 1.1, 1.0, 1.2, 1.2\}$
$\Lambda = \text{diag}\{2.0, 2.0, 3.5, 1.5, 1.5, 1.2, 3.0, 3.0\}$
$\bar{M} = \text{diag}\{2, 2, 2, 0.02, 0.02, 0.02, 0.05, 0.05\}$
$\hat{\sigma}(0) = 0.1, \nu = 2.0$

4) *Evaluation Scenarios*: To rigorously assess the framework across varying dynamic regimes, we define a centralized set of physical testing scenarios (cf. Fig. 4). The evaluation comprises two distinct trajectories: *Scenario A* executes an altitude-varying S-shaped pick-and-place maneuver, grasping an object from a 10 cm high box and placing it onto a 55 cm high table, which heavily excites vertical regime shifts and ground-effect transients. *Scenario B* entails a continuous Figure-8 trajectory, picking and placing the object strictly on the 55 cm table maintaining same height, designed to induce continuous roll-pitch.

Joints of the manipulator moves in the range  $(-20.1^\circ, 37.2^\circ)$  and  $(65.3^\circ, 77.2^\circ)$  respectively during the pick-and-place maneuver.

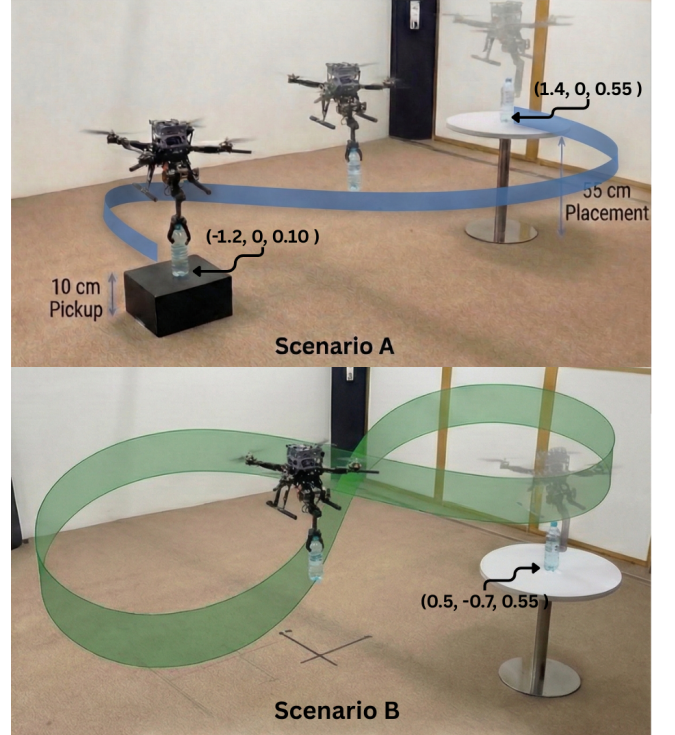


Fig. 4: Dynamic evaluation scenarios. (Top) **Scenario A**: An altitude-varying S-shaped pick-and-place maneuver. (Bottom) **Scenario B**: A continuous Figure-8 trajectory. Unit of coordinates in the figure is in meters.

#### B. Model Validation: Open-Loop Prediction Accuracy

For predictive accuracy evaluation, the quadrotor tracks a smooth reference trajectory using a vanilla PID controller for 5 min with a payload of 300 g is attached to end-effector while  $\mathbf{r}$  is computed at each timestep from (2). Performance is quantified via Root Mean Squared Error (RMSE) in residual predictions alongside the Coefficient of Determination ( $R^2$ ) to evaluate variance capture and record

TABLE II: Model prediction performance comparison

Method	RMSE ↓	R <sup>2</sup> ↑	Inf. (ms)
SysID [23]	1.363	0.207	0.01
GP [10]	0.84	0.493	17.20
LSTM [24]	0.76	0.576	1.20
Transformer [25]	0.67	0.623	4.10
Neural-fly [16]	0.48	0.761	9.50
MLP (last layer) [17]	0.41	0.802	4.50
FDT (Base)	0.29	0.912	1.86
<b>FDT + LRA (Ours)</b>	<b>0.21</b>	<b>0.972</b>	<b>3.02</b>

the mean inference time in *milliseconds* (Inf. (ms)), as shown in Table II.

### C. Trajectory Tracking & Disturbance Rejection

We evaluate trajectory tracking performance, for scenarios A and B and shown in Fig. 4, by applying the control law (22) and computing the root-mean-square error (RMSE) of error signal  $e(t)$  for each method. Table III Shows the performance of compared baselines under same testing scenarios.

### D. Analysis

As evidenced by Tables II and III, across both prediction and tracking metrics, performance correlates with how explicitly each method models structured residual dynamics and adapts to time-varying system dynamics. Sparse identification methods are constrained by predefined functional libraries, leading to systematic bias under strongly coupled inertial and aerodynamic effects. GP models capture smooth disturbances but struggle with scalability and high-dimensional coupling. Sequence models such as LSTM and Transformer architectures mitigate temporal compounding error; however, recurrent memory or time-tokenized attention alone entangles instantaneous dynamics with slow regime evolution, limiting structural interpretability and generalization.

While  $\mathcal{L}_1$ -adaptive control ensures robustness under bounded matched uncertainties, it lacks an explicit residual model, causing performance degradation under structured, configuration-dependent multiscale dynamics. Adaptive model learning approaches improve the model performance, but their mechanisms differ fundamentally. Meta-learned models such as Neural-Fly rely on interpolation within trained task families and lack explicit structural decomposition of residual components, restricting extrapolation under abrupt inertial changes. Gradient-based last-layer updates adapt parameters in weight space, coupling representation and identification and resulting in slower, optimizer-sensitive convergence. In contrast, our framework constrains adaptation to a linear latent subspace with closed-form updates, yielding well-conditioned, rapid regime adaptation while preserving structured residual representation. Notably, FDT+LRA preserves millisecond-scale inference, indicating that structured factorization and latent adaptation impose minimal computational overhead in real-time operation.

### E. Ablation Studies

To validate the architectural design, we perform ablation studies on our model, in Scenario B under a 500 g payload and 1.0 m/s mean velocity, we use model prediction RMSE to compare the degraded model with proposed full model (percentage  $\Delta$  RMSE vs. Full) quantifying the impact on predictive accuracy, shown in Table IV.

The ablation results confirm that structured multi-scale factorization is critical for accurate residual modeling. Removing the long-horizon memory or short-horizon context encoding leads to the largest degradation, indicating that both slow regime evolution and instantaneous cross-variable coupling are indispensable for capturing AAM residual dynamics under payload variation. Eliminating the global token significantly impairs performance, demonstrating that explicit cross-variable aggregation is essential for coherent latent regime representation. Finally, disabling the online LRA produces a moderate but consistent degradation, verifying that latent-space adaptation enhances robustness under regime shifts while relying on the structural backbone of the full FDT.

## IV. CONCLUSION AND FUTURE WORK

We introduced a predictive-adaptive framework for compensating nonstationary residual dynamics in aerial manipulators. The proposed Factorized Dynamics Transformer structurally separates cross-variable inertial coupling from long-horizon aerodynamic memory, enabling accurate multi-scale residual prediction. A Latent Residual Adapter performs lightweight online linear identification in latent space, allowing rapid recovery from unseen payload shifts while preserving real-time feasibility. Real-world experiments demonstrate improved prediction accuracy, faster disturbance rejection, and superior closed-loop tracking compared to classical and learning-based baselines, underscoring the value of structured factorization and continuous latent adaptation for robust aerial manipulation.

The proposed factorization and latent linear adaptation assume that regime shifts remain locally linearizable in the learned latent representation in the learned representation, which may break down under highly abrupt or extreme dynamic transitions. Future work will incorporate uncertainty-aware residual modeling and explicit transient regime-change detection to improve adaptation beyond the initial training envelope.

## REFERENCES

- [1] F. Ruggiero, V. Lippiello, and A. Ollero, "Aerial manipulation: A literature review," *IEEE Robotics and Automation Letters*, vol. 3, no. 3, pp. 1957–1964, 2018.
- [2] A. Suarez, V. M. Vega, M. Fernandez, G. Heredia, and A. Ollero, "Benchmarks for aerial manipulation," *IEEE Robotics and Automation Letters*, vol. 5, no. 2, pp. 2650–2657, 2020.
- [3] M. Orsag, C. Korpela, P. Oh, S. Bogdan, and A. Ollero, *Aerial Manipulation*. Springer, 2018.
- [4] A. Ollero, M. Tognon, A. Suarez, D. Lee, and A. Franchi, "Past, present, and future of aerial robotic manipulators," *IEEE Transactions on Robotics*, vol. 38, no. 1, pp. 626–645, 2022.
- [5] X. Meng, Y. He, and J. Han, "Survey on aerial manipulator: System, modeling, and control," *Robotica*, vol. 38, no. 7, pp. 1288–1317, 2020.

TABLE III: Tracking RMSE under In-Distribution (300 g) and Out-of-Distribution (500 g) payloads for Scenario A and Scenario B.

Method	Scenario A				Scenario B			
	In-Distribution (300 g)		Out-of-Distribution (500 g)		In-Distribution (300 g)		Out-of-Distribution (500 g)	
	Slow (0.5 m/s) ↓	Fast (1.0 m/s) ↓	Slow (0.5 m/s) ↓	Fast (1.0 m/s) ↓	Slow (0.5 m/s) ↓	Fast (1.0 m/s) ↓	Slow (0.5 m/s) ↓	Fast (1.0 m/s) ↓
<i>Baseline</i>								
$\mathcal{L}_1$ Adaptive [26]	1.222	1.560	1.711	2.223	0.981	1.202	1.293	1.617
<i>Offline learning Baselines</i>								
GP [10]	0.752	0.960	1.053	1.368	0.604	0.740	0.796	0.995
LSTM [24]	0.680	0.868	0.952	1.237	0.546	0.669	0.720	0.900
GPT-2 [27]	0.599	0.765	0.839	1.090	0.481	0.589	0.634	0.793
<i>Online adaptation Baselines</i>								
Neural-fly [16]	0.429	0.547	0.600	0.780	0.344	0.422	0.454	0.567
MLP (last layer) [17]	0.366	0.467	0.512	0.665	0.294	0.360	0.387	0.484
<b>Ours</b>								
<b>FDT (Ours)</b>	0.258	0.330	0.362	0.470	0.207	0.254	0.274	0.342
<b>FDT+LRA (Ours)</b>	<b>0.215</b>	<b>0.275</b>	<b>0.301</b>	<b>0.391</b>	<b>0.173</b>	<b>0.212</b>	<b>0.228</b>	<b>0.285</b>

TABLE IV: Ablation Study on Test Set

Variant	RMSE ↓	$\Delta$ RMSE vs. Full(%)
<b>FDT - Full + LRA</b>	<b>0.283</b>	–
w/o Online LRA (II-B.1)	0.37	+30.7%
w/o Global Token (g)	0.692	+144.5%
w/o Short-Horizon Context Encoding (II-A.2)	0.778	+174.9%
w/o Long-Horizon Memory (II-A.3)	0.782	+176.3%

- [6] A. Saviolo and G. Loianno, “Learning quadrotor dynamics for precise, safe, and agile flight control,” *Annual Reviews in Control*, vol. 55, pp. 45–60, 2023.
- [7] T. Z. Jiahao, K. Y. Chee, and M. A. Hsieh, “Online dynamics learning for predictive control with an application to aerial robots,” in *Conference on Robot Learning*. PMLR, 2023, pp. 2251–2261.
- [8] G. Shi, X. Shi, M. O’Connell, R. Yu, K. Azizzadenesheli, A. Anandkumar, Y. Yue, and S.-J. Chung, “Neural lander: Stable drone landing control using learned dynamics,” in *2019 International Conference on Robotics and Automation (ICRA)*. IEEE, 2019, pp. 9784–9790.
- [9] T. Salzmann, E. Kaufmann, J. Arrizabalaga, M. Pavone, D. Scaramuzza, and M. Ryll, “Real-time neural mpc: Deep learning model predictive control for quadrotors and agile robotic platforms,” *IEEE Robotics and Automation Letters*, vol. 8, no. 4, pp. 2397–2404, 2023.
- [10] G. Torrente, E. Kaufmann, P. Föhn, and D. Scaramuzza, “Data-driven mpc for quadrotors,” *IEEE Robotics and Automation Letters*, vol. 6, no. 2, pp. 3769–3776, 2021.
- [11] W. Cao, A. Capone, R. Yadav, S. Hirche, and W. Pan, “Computation-aware learning for stable control with gaussian process,” in *Proceedings of Robotics: Science and Systems (RSS)*, 2024.
- [12] A. Saviolo, G. Li, and G. Loianno, “Physics-inspired temporal learning of quadrotor dynamics for accurate model predictive trajectory tracking,” *IEEE Robotics and Automation Letters*, vol. 7, no. 4, pp. 10 256–10 263, 2022.
- [13] N. Mohajerin and S. L. Waslander, “Multistep prediction of dynamic systems with recurrent neural networks,” *IEEE Transactions on Neural Networks and Learning Systems*, vol. 30, no. 11, pp. 3370–3383, 2019.
- [14] F. Djeumou, C. Neary, and U. Topcu, “How to learn and generalize from three minutes of data: Physics-constrained and uncertainty-aware neural stochastic differential equations,” in *Conference on Robot Learning*. PMLR, 2023, pp. 577–601.
- [15] A. Das, R. D. Yadav, S. Sun, M. Sun, S. Kaski, and W. Pan, “Dronediffusion: Robust quadrotor dynamics learning with diffusion models,” in *2025 IEEE International Conference on Robotics and Automation (ICRA)*. IEEE, 2025, pp. 1604–1610.
- [16] M. O’Connell, G. Shi, X. Shi, K. Azizzadenesheli, A. Anandkumar, Y. Yue, and S.-J. Chung, “Neural-fly enables rapid learning for agile flight in strong winds,” *Science Robotics*, vol. 7, no. 66, p. eabm6597, 2022.
- [17] A. Saviolo, J. Frey, A. Rathod, M. Diehl, and G. Loianno, “Active learning of discrete-time dynamics for uncertainty-aware model predictive control,” *IEEE Transactions on Robotics*, vol. 40, pp. 1273–1291, 2024.
- [18] A. Gahlawat, P. Zhao, A. Patterson, N. Hovakimyan, and E. Theodorou, “L1-gp: L1 adaptive control with bayesian learning,” in *Learning for dynamics and control*. PMLR, 2020, pp. 826–837.
- [19] T. Lew, A. Sharma, J. Harrison, A. Bylard, and M. Pavone, “Safe active dynamics learning and control: A sequential exploration–exploitation framework,” *IEEE Transactions on Robotics*, vol. 38, no. 5, pp. 2888–2907, 2022.
- [20] S. Richards, N. Azizan, J.-J. Slotine, and M. Pavone, “Adaptive-control-oriented meta-learning for nonlinear systems,” in *Robotics: Science and Systems*, 2021.
- [21] M. Orsag, C. Korpela, S. Bogdan, and P. Oh, “Dexterous aerial robots—mobile manipulation using unmanned aerial systems,” *IEEE Transactions on Robotics*, vol. 33, no. 6, pp. 1453–1466, 2017.
- [22] D. Mellinger and V. Kumar, “Minimum snap trajectory generation and control for quadrotors,” in *2011 IEEE International Conference on Robotics and Automation (ICRA)*. IEEE, 2011, pp. 2520–2525.
- [23] E. Kaiser, J. N. Kutz, and S. L. Brunton, “Sparse identification of nonlinear dynamics for model predictive control in the low-data limit,” *Proceedings of the Royal Society A*, vol. 474, no. 2219, p. 20180335, 2018.
- [24] P. P. Rao, A. Saviolo, T. C. Ferrari, and G. Loianno, “Learning long-horizon predictions for quadrotor dynamics,” in *2024 IEEE/RSJ International Conference on Intelligent Robots and Systems (IROS)*. IEEE, 2024, pp. 12 758–12 765.
- [25] A. Vaswani, N. Shazeer, N. Parmar, J. Uszkoreit, L. Jones, A. N. Gomez, Ł. Kaiser, and I. Polosukhin, “Attention is all you need,” *Advances in neural information processing systems*, vol. 30, 2017.
- [26] Z. Wu, S. Cheng, P. Zhao, A. Gahlawat, K. A. Ackerman, A. Lakshmanan, C. Yang, J. Yu, and N. Hovakimyan, “L 1 quad: L 1 adaptive augmentation of geometric control for agile quadrotors with performance guarantees,” *IEEE Transactions on Control Systems Technology*, vol. 33, no. 2, pp. 597–612, 2025.
- [27] L. Chen, K. Lu, A. Rajeswaran, K. Lee, A. Grover, M. Laskin, P. Abbeel, A. Srinivas, and I. Mordatch, “Decision transformer: Reinforcement learning via sequence modeling,” *Advances in Neural Information Processing Systems*, vol. 34, pp. 15 084–15 097, 2021.